Quantitative analysis of the aqueous fraction from the Fe-assisted hydrothermal liquefaction of oil palm empty fruit bunches

Miyata, Yoshinori
Yamazaki, Yoshiko
Hirano, Yoshiaki
Kita, Yuichi

(Citation)
Journal of Analytical and Applied Pyrolysis,132:72-81

(Issue Date)
2018-06

(Resource Type)
journal article

(Version)
Accepted Manuscript

Quantitative analysis of the aqueous fraction from the Fe-assisted hydrothermal liquefaction of oil palm empty fruit bunches

Yoshinori Miyata,[a,b] *Yoshiko Yamazaki,*[b] *Yoshiaki Hirano,*[b*] *and Yuichi Kita*[b]

[a] New Business Planning Department, Nippon Shokubai Co., Ltd., Suita, Osaka 564-8512, Japan

[b] Department of Chemical Science and Engineering, Graduate School of Engineering, Kobe University, Kobe 657-8501, Japan

Email ID of Authors:

Yoshinori Miyata (Yoshinori_Miyata@shokubai.co.jp); Yoshiko Yamazaki (yamazaki@panda.kobe-u.ac.jp); Yoshiaki Hirano (hirano@phoenix.kobe-u.ac.jp) ;Yuichi Kita (yuichi_kita@lion.kobe-u.ac.jp)

* **Corresponding author.**

Yoshiaki Hirano,
Department of Chemical Science and Engineering,
Graduate School of Engineering,
Kobe University,
Kobe 657-8501, Japan
TEL: +81-78-803-6512
Email: hirano@phoenix.kobe-u.ac.jp

Abstract

Hydrothermal liquefaction is a promising candidate method for the conversion of biomass resources. To improve economic efficiency, the development of processes that utilize the water-soluble (WS) hydrothermal-liquefaction fraction is critical; consequently, a fundamental method for the analysis of the WS fraction is required. In this study, the quantitative analysis of the WS fraction obtained from the Fe-assisted hydrothermal liquefaction of oil palm empty fruit bunches was comprehensively investigated by combining various separation and analysis methods. The volatile components of the WS fraction were analyzed by gas chromatography–mass spectrometry (GC–MS) and gas chromatography–flame ionization detection (GC–FID), and they were quantified using the relative response factors estimated by the effective carbon number method. Heavy components not detectable by GC were isolated by freeze-drying, and their elemental compositions, functional groups, and molecular-weight distributions were analyzed. The results reveal that the addition of Fe during hydrothermal liquefaction alters the types of compounds present in the WS fraction by a large extent, and increases the proportion of volatile compounds. The reactivity of the WS fraction in the zeolite-catalyzed cracking reaction was also investigated, which revealed that the volatile components of the WS fraction are efficiently converted into olefins.

Keywords : Hydrothermal liquefaction, Iron, Aqueous fraction, Relative response factor, Effective carbon number, Freeze-dry

1. Introduction

The effective utilization of biomass resources, such as agricultural residues, algae, and sewage sludge, is an urgent and important issue that will help society prepare for the depletion of fossil-based resources in the future. Fast pyrolysis and hydrothermal liquefaction reactions have been extensively studied as methods for the liquefaction of biomass resources and their subsequent use as fuels and chemical feedstocks [1, 2]. The hydrothermal liquefaction reaction is a promising method for the liquefaction of biomass, and operates at moderate temperatures (280–370 °C) and high pressures (10–25 MPa) [3-6]. During this process, ubiquitous water is used as the solvent, which is advantageous since wet biomass can be used without any pre-drying. The product of the hydrothermal liquefaction reaction is separated into four fractions, namely water-soluble (WS) and water-insoluble (WI) fractions, as well as solid residues (SRs), and gases (Figure 1) [7]. Increasing the levels of the WS and WI fractions, which can be used as fuels and chemical feedstocks, is important in order to improve biomass-utilization efficiency. Until now, the WI fractions (biocrudes) have largely been regarded as useful resources and the focus of analytical research has almost exclusively been directed toward these fractions; however, the use of the WS fraction also needs to be considered as a possible strategy in this regard [8-13].

Recently, we demonstrated the hydrothermal liquefaction of palm empty fruit bunches (EFBs) and demonstrated that the use of Fe-metal powder, as an additive, considerably increased the yield of the WS fraction [14]. In addition, catalytic cracking of the WS fraction over a solid acid catalyst (HZSM-5 zeolite) afforded hydrocarbons, such as olefinic and aromatic compounds, that can be used as basic chemical raw

materials. During the cracking reaction, the WS fraction obtained from the Fe-assisted hydrothermal system contained higher levels of hydrocarbon products than that obtained from a conventional hydrothermal system, revealing that Fe not only accelerates decomposition, but also affords more upgraded products. Preliminary analysis of the WS fraction revealed that the product composition had changed significantly following addition of Fe. However, further analysis of the WS fraction was difficult due to its complex composition; consequently, only a qualitative discussion on the effect of Fe was provided. In order to clarify the role of Fe, optimize the hydrothermal decomposition process, and develop methods that use the WS fraction, a rapid and accurate method for the evaluation of the WS fraction is a key technological objective.

Reports on the analysis of the aqueous fractions from the hydrothermal liquefaction of biomass have been published; however, quantitative analyses are limited to only a few cases [15-19]. As analytical methods, gas chromatography–mass spectrometry (GC–MS) and gas chromatography–flame ionization detection (GC–FID) are often used; these methods are powerful because they can rapidly analyze multicomponent mixtures. For quantitative analysis by GC, the preparation of calibration curves using authentic samples is necessary. The analysis of complex mixtures, such as those from the thermochemical decomposition of biomass, is labor-intensive and costly. In particular, when no standard reagents are on hand, and when they cannot be easily purchased, it becomes necessary to synthesize authentic samples, which is not a realistic approach for trace amounts of product.

Even when standards are not available, relative response factors (RRFs) of analytes for FID analysis can

be estimated from the chemical structures of the analytes; consequently, calibration curves can still be prepared. Sternberg et al. proposed a method for predicting the RRF of a compound bearing heteroatoms by introducing the concept of effective carbon number (ECN) [20]. They showed that the effect of heteroatoms on the ECN of a molecule depended on the nature of the functional groups and empirically quantified the contribution of each functional group to the ECN. A number of studies on predicting RRF have been reported [21-24], and the predicted RRFs have been shown to be useful for the analysis of scent [25] and taste [26], and in other areas [27]. Biomass-derived components produced by thermochemical conversion were also analyzed using predicted RRFs [28-31]. For example, Undri et al. successfully quantified the composition of the biocrude obtained by rapid pyrolysis using an independently developed RRF prediction method [32].

In this study, we developed a modified technique for predicting ECN based on the above-mentioned method, quantitatively analyzed the crude WS fraction from the hydrothermal liquefaction of biomass, and clarified the composition of the volatile components. In addition, we introduce a freeze-drying method [33, 34] and succeeded in isolating non-volatile WS components that cannot be detected by GC. The compositions and properties of the isolated heavy components were determined by elemental analysis, Fourier-transform infrared spectroscopy (FT-IR) and gel-permeation chromatography (GPC). Combining these methods has enabled the comprehensive analysis of the WS fraction and a detailed discussion of the effect of the Fe additive. In addition, by examining the cracking characteristics of the volatile and heavy components of the WS fraction, guidelines for the optimization of the hydrothermal liquefaction process

are proposed.

2. Materials and Methods

2.1. Materials

Oil palm empty fruit bunches (EFBs) from Indonesia were supplied by the Nippon Shokubai Co., Ltd. (Japan), and were used as the lignocellulosic-biomass feedstock. The EFBs were dried at 25 °C and crushed into particles less than 300 μm in size. Fe powder (99.9%, NM-0029-UP) was purchased from Ionic Liquids Technologies GmbH (Germany). HZSM-5 zeolite with a Si/Al ratio of 24:1 was supplied by the Nippon Shokubai Co., Ltd. (Japan). Internal standards and authentic samples for GC analyses were obtained commercially. 2-Methoxyethanol, cyclopentanone, 1-hydroxy-2-propanone, propanol, acetic acid, propanoic acid, cyclopentanol, cyclohexanol, propyleneglycol, 1,2-ethanediol, 1,2-butanediol, 1,4-butanediol, 1,2-pentanediol, 1,2-hexanediol, 1,2-cyclohexanediol, 4-oxopentanoic acid, furfural, phenol, methyl *p*-hydroxybenzoate, cinnamaldehyde, and 3-phenyl-2-propen-1-ol from purchased from Wako Pure Chemical Industries, Ltd., while cyclohexanone, 3-hydroxy-2-butanone, methyl DL-2-hydroxy-3-butenoate, 2-butanone, 2,3-butanediol, *tert*-butyl alcohol, *tert*-amyl alcohol, 5-hydroxymethyl-2-furaldehyde, guaiacol, syringol, syringaldehyde, and vanillin were purchased from Tokyo Chemical Industry Co., Ltd.

2.2. Preparation of the WS fraction

EFB liquefaction and separation experiments were conducted following a previously published method [14]. Briefly, EFB (4.0 g), Fe powder (0 or 6.256 g), and H_2O (40 g) were introduced into a Hastelloy C high-pressure reactor, which was purged four times with nitrogen. The initial pressure was set to 1.0 MPa with nitrogen, and the stirring rate was adjusted to 700 rpm. The reactor was then heated to 300 ℃ and maintained at this temperature for 10 min. The reactor was then rapidly cooled to 25 ℃ using ice-water. The reaction mixture was filtered and the filtrate was collected as the WS fraction. The total organic carbon (TOC) content of the WS fraction was determined using a total organic carbon analyzer (Shimadzu, TOC-LCSH/CSN). The pH of the WS fraction was measured with a LAQUAtwin B-711 pH analyzer (HORIBA). Sample information is summarized in Table 1. Each reaction was carried out in quadruplicate and product yields were calculated as averages.

2.3. Gas Chromatographic analysis of the WS fraction

The WS fraction sample was diluted with acetone (1:1 v/v) and 2-methoxyethanol (0.05 wt%) was added as an internal standard. Samples were analyzed by gas chromatography–mass spectrometry (GC–MS) on a Shimadzu QP-2010 system equipped with a capillary column (GL Sciences, Inert-cap® WAX-HT, 30 m × 0.25 mm ID × 0.25 μm film thickness), and gas chromatography (Shimadzu, GC-2014) using the same capillary column described above, but equipped with a flame ionization detector (GC–FID). The split ratio was set to 1:50 and the injection volume was 1.0 μL. The oven was operated at 50 ℃ for 3 min, then heated at 10 ℃/min to 260 ℃, and maintained at this temperature for 16 min; the total run time was 30

min. All compounds were identified by comparing their mass spectra with those from the National Institute of Standards and Technology (NIST) library of mass spectral data. When authentic samples were available, product retention times were confirmed to coincide with those of the authentic samples.

2.4. Quantitative GC–FID method

Quantitative calculations based on the GC–FID data were carried out using relative response factors (RRFs). The RRF is defined by eq. 1 [35]:

$$\mathrm{RRF} = \frac{A_i \times C_{IS}}{C_i \times A_{IS}} \quad (1),$$

where "*C*" is the concentration, "*A*" is the peak area, and the subscripts "*i*" and "*IS*" refer to the analyte and internal standard, respectively.

The concentration of the analyte can be calculated from eq. 2:

$$C_i = C_{IS} \times \frac{A_i}{A_{IS}} \times \frac{1}{\mathrm{RRF}} \quad (2),$$

where the RRF was obtained by eq. 1 for compounds that are available as authentic sample; quantitative analysis is then carried out according to eq. 2.

On the other hand, the relationship between RRF and the effective carbon number (ECN) is given by eq. 3 [24]:

$$\mathrm{RRF} = \frac{\mathrm{ECN_i} \times \mathrm{MW_{IS}}}{\mathrm{MW_i} \times \mathrm{ECN_{IS}}} \quad (3).$$

From eqs. 2 and 3, the concentration of an analyte (C_i) can be calculated if the ECN of each compound in the analytical sample can be determined. Based on Sternberg's concept, the ECN can be determined using

the following equation [36]:

$$\mathrm{ECN} = \sum_{k} (\mathrm{N}_k \times \mathrm{Cnt}_k) \quad (4),$$

where “N” is the number of atoms or functional groups in the compound and “Cnt” is the ECN contribution coefficient, which is an empirical factor. Cnt values have been summarized by Sternberg et al.; however, there are differences between the calculated and measured RRF values since response depends subtly on equipment and conditions. In order to correct for this difference, authentic samples were selected and mixtures of known concentrations of authentic samples and internal standards were analyzed. Cnt values were recursively optimized to give the best correlation between predicted and measured RRF values.

2.5. Freeze-dry separation of the WS fraction and subsequent analysis

The freeze-drying apparatus was assembled using a round-bottom flask, glass adapters, a vacuum trap, manometer, and vacuum pump (Figure 2). The crude WS fraction sample (10 mL) was placed in the round-bottom flask, after which it was rapidly frozen by immersing the flask in liquid nitrogen. The frozen samples were immediately connected to the apparatus and maintained under vacuum (< 0.2 kPa) for 5 h. Sublimated water and volatile compounds were collected in a cold trap cooled by liquid nitrogen.

The moisture content of the residue in the flask was determined using a Karl Fischer moisture titrator (MKV-710, Kyoto Electronics Manufacturing Co., Ltd.); AQUAMICRON® Titrant SS 3mg and AQUAMICRON® Solvent CP (Mitsubishi Chemical Corporation) were used for titration. Elemental

analysis (CHN) of the freeze-dried WS-fraction sample was performed using an elemental analyzer (Elementar Vario EL cube) and sulfanilamide as the calibration standard. The oxygen mass content was calculated by difference. The FT-IR spectrum (KBr smear) of the freeze-dried WS-fraction sample was acquired on a Thermo Nicolet NEXUS 670 Fourier-transform infrared spectrometer operating in transmission mode between 4000 and 400 cm^{-1}. The sample was dried under vacuum to remove water. Gel-permeation chromatography (GPC) of the dried WS-fraction samples was performed using a TOSOH HLC-8320GPC GPC system equipped with a refractive index detector and fitted with a series of four TOSOH TSKgel SuperH2000 columns (3 μm, 150 mm × 6 mm ID). Before analysis, the sample was dissolved in tetrahydrofuran (THF) and filtered through a 0.45 μm syringe filter. Chromatograms were recorded at 40 °C over 30 min using THF as the eluent at a rate of 0.6 mL/min. Polyethylene glycol was used as the molecular-weight calibration standard.

2.6. Catalytic cracking of the WS fraction and subsequent analysis

Catalytic cracking of the WS fraction was performed following a previously published method using a fixed-bed continuous flow reactor composed of a stainless-steel tube reactor, gas-feeding system, liquid-feeding pump, heating system, gas wash bottle filled with ice-cold water, and a gas sampling system [14]. HZSM-5 zeolite (3.3 g, spherical, with particle diameters of 0.85–1.7 mm) was added to the reactor, followed by the addition of stainless-steel beads for liquid-feedstock vaporization. The catalyst was flushed with nitrogen (50 mL/min) for 1 h at 25 °C, followed by heating to 600 °C under nitrogen (50 mL/min).

The WS fraction was fed into the reactor using a plunger pump at a weight hourly space velocity (WHSV) of 1.1 h^{-1}. During the reaction, the condensed products were collected using a gas wash bottle with either water or acetonitrile. All gaseous products were collected in a gas-sampling bottle. Gaseous products were analyzed using two gas chromatography systems: a Shimadzu GC-8A chromatograph equipped with silica-gel (Shinwa Chemical Industries, ZS-74) and 5A-molecular-sieve (Shinwa Chemical Industries, ZM-1) columns, and a thermal conductivity detector for CO_2 and CO, and a Shimadzu GC-2014 instrument equipped with a Sunpak-A column (Shinwa Chemical Industries, ZS-72) and a flame ionization detector for hydrocarbons.

2.7. Product yield

The yields from hydrothermal liquefaction and catalytic cracking were calculated as follows:

$$\text{Yield of each fraction from hydrothermal liquefaction (\%)} = \frac{\text{Moles of carbon in the product}}{\text{Moles of carbon in the raw material}} \times 100 \quad (5), \text{ and}$$

$$\text{Yield of each product from catalytic cracking (\%)} = \frac{\text{Moles of carbon in the product}}{\text{Moles of carbon in the WS-feed fraction}} \times 100 \quad (6).$$

3. Results and Discussion

3.1. GC analysis of the WS fraction

3.1.1. Predicting the RRF

As reported in our previous work, the WS fraction produced by hydrothermal liquefaction contained functionalized aliphatic compounds such as alcohols, ketones, and carboxylic acids, among others. In order to determine the influence of the functional groups borne by these compounds on the ECN, 14 parameters (three elements (C, H, O) and 11 functional groups) were used in eq. 4. To optimize the Cnt value, 32 authentic samples were selected; these samples were either present in the WS fraction or had similar compositions to those present. The RRFs of the authentic samples (RRF_{found}) were calculated using eq. 1 and experimental data. Cnt values were optimized recursively so that the RRF values calculated from eqs. 3 and 4 (RRF_{calc}) were close to the values of RRF_{found}. The data were optimized using the "solver" plug-in of Excel® (Microsoft Corp.) [32]. Cnt, RRF_{found}, and RRF_{calc} values are summarized in Table 2. Figure 3 reveals a good linear relationship between RRF_{calc} and RRF_{found}, with a correlation coefficient (R^2) of 0.9859. Even when no authentic sample is available and a calibration curve cannot be created, it is now possible to calculate the RRF of a compound from its chemical structure in order to perform quantitative analyses.

3.1.2. Quantitative GC analysis of the WS fraction

The crude WS fractions obtained by the hydrothermal liquefaction of the EFB in the presence and absence of Fe were analyzed by GC–MS. Compounds were identified from their MS fragmentation patterns by comparisons with spectra in the NIST database. The light WS components were quantified using the

RRF_{found} and RRF_{calc} values, the results of which are summarized in Table 3. Furthermore, the carbon yields (eq. 5) were grouped according to compound classification, as showed in Figure 4.

We previously detected hydroxyketones, such as hydroxyacetone or 3-hydroxy-2-butanone, as characteristic compounds in Fe-assisted hydrothermal liquefaction reactions. The yield of hydroxyketones in the Fe-assisted WS fraction was quantified to be 12.9%, which represents half of the total yield of identified compounds. The yields of simple alcohols and ketones were determined to be 1.4% and 5.7% respectively. With the exception of acetic acid, carboxylic acids were hardly detected; their acidities are frequently problematic properties of thermal decomposition products. This result is consistent with the observation that the Fe-assisted WS fraction exhibited relatively mild acidity (Table 1). The total yield of identified products was 28.6%, which is half of the crude WS fraction yield.

On the other hand, fewer product peaks were detected in the WS fraction produced by conventional hydrothermal decomposition compared to those from the Fe-assisted process; the total product yield was determined to be 10.0%, which represents one third of the total WS fraction yield. The low proportion of GC-quantifiable components in the crude WS fraction indicates that this fraction has overall low volatility. The major compounds were carboxylic acids, mainly acetic acid; the pH value of 3.4 is also consistent with an abundance of acids (Table 1).

The yields of phenols are low in both processes; it seems that lignin cannot be decomposed to its phenylpropanoid monomeric units in this reaction system.

As shown above, the effect of Fe on the yields of light WS products can be evaluated quantitatively.

3.2. Insight into the heavy WS components

3.2.1. Separation of the heavy WS components

It was only possible to detect and quantify the light WS components by GC; however, in order to clarify the composition of the entire WS fraction, information on the remaining heavy WS components must be obtained. Since water and the light WS components are analysis obstacles, determination of only the heavy WS components is difficult. Therefore, we attempted to remove water and the low molecular-weight compounds from the crude WS fraction. Since distillation or evaporation would add thermal history to the sample, there is a decomposition risk to the WS fraction; consequently, we chose to use the freeze-drying method. The liquid-nitrogen-frozen crude WS fraction was evacuated to a pressure below 0.2 kPa at room temperature. After the water had sublimed, a viscous residue remained in the bottom of the flask, as shown in Figure 5 (freeze-dried bottom, FDB). The sublimed water and other volatile compounds were collected in a liquid-nitrogen trap and recovered as a clear aqueous solution (volatile fraction, VF). The mass balances before and after separation were consistent, and the carbon yield was confirmed by TOC measurements (Table 4); the carbon yield of the VF was determined to be 52% and 32% for the Fe-assisted and conventional hydrothermal WS fractions, respectively, which is in agreement with the carbon-yield proportion of the light WS components in the crude WS fraction determined by GC. In addition, the gas chromatogram of each VF was almost identical to that of the crude WS fraction, whereas the corresponding chromatograms of the FDB exhibited peaks that were significantly lower in intensity than

those observed for the crude WS fractions (Figure 6). Furthermore, the Karl Fischer method also confirmed that the moisture contents of the residues were less than 5%. We conclude from these results that the light WS components and water were separated by freeze-drying in the VF, while heavy WS components were condensed in the FDB.

3.2.2. Elemental composition of the WS fraction

Elemental compositions of the light WS components were calculated by counting the elements in each GC-quantified compound. Elemental compositions of the heavy WS components were quantified by elemental analyses of the FDBs (the influences of residual moisture and the light WS components were subtracted). Elemental compositions of the crude WS fractions were calculated by combining the light and heavy WS elemental compositions by considering the proportion of each components. The results are displayed in the forms of H/C and O/C ratios mapped on a van Krevelen diagram and compared with those of biomass feedstocks such as raw EFBs, cellulose, hemicellulose, lignin, as well as biomass-derived chemicals and petrochemicals (Figure 7) [37].

The diagonal lines in the diagram are hydrogen-to-carbon effective-ratio (H/C_{eff}) contour lines (eq. 7), which are often used to estimate and describe biomass upgrading [38]. To bring the elemental composition of biomass-derived compounds close to those of petrochemicals, oxygen should be removed in the form of H_2O; consequently, one mole of oxygen reduces two moles of effective hydrogen, as shown in eq. 7. A higher H/C_{eff} value indicates more efficient reforming during this process.

$$H/C_{eff} = \frac{[H]-2[O]}{[C]} \quad (7).$$

We found that the H/C ratio was higher and the O/C ratio was lower when the sample was prepared in the presence of Fe. The crude WS fraction prepared by conventional hydrothermal liquefaction had a similar composition to cellulose or hemicellulose, the H/C_{eff} of which was almost zero. The H/C and O/C ratios apparently improved by employing Fe as an additive, with the H/C_{eff} increasing to 0.57. These results suggest that Fe is capable of hydrodeoxygenating the sample, which effectively improves the hydrothermal liquefaction reaction. Huber et al. demonstrated the two-step hydrodeoxygenation of the aqueous fraction extracted from a pyrolysis oil [39]. The extracted aqueous fraction of the pyrolysis oil (water-soluble fraction of pinewood bio-oil, WSBO) has a composition close to that of the WS fraction obtained by hydrothermal liquefaction since their H/C_{eff} ratios are similar; the H/C_{eff} of the WSBO increased from 0.14 to 0.71 by ruthenium-catalyzed hydrodeoxygenation. Hence, our one-step Fe-assisted hydrothermal liquefaction process is nearly equivalent to this two-step system. However, when compared to other biomass-derived chemicals and petrochemicals, the H/C_{eff} ratio is still low. Improvement in the reaction conditions during Fe-assisted hydrothermal liquefaction, or the development of an additional upgrading catalyst, is required to increase the efficiency of this process.

3.2.3. FT-IR spectrum of the freeze-dried WS fraction

The FDB samples were examined by FT-IR spectroscopy in order to obtain information on the functional groups present in the heavy WS components; the IR spectra are shown in Figure 8.

The heavy WS components were presumed to contain complicated mixtures since few sharp peaks attributable to specific functional groups are observed in the spectra. Broad strong absorptions were observed at around 3400 cm^{-1} in both samples, consistent with the presence of OH groups (and residual water) [40]. These OH groups originate from cellulose and hemicellulose, and the water-solubilities and non-volatilities of the heavy WS components are due to these groups. A shoulder observed at around 2500 cm^{-1} in the conventional hydrothermally liquefacted sample indicates the intermolecular hydrogen bonding of carboxylic acid [41], suggesting that COOH groups are more abundant in this sample than in that produced by Fe assistance. The peaks observed between 3000 and 2800 cm^{-1} in both samples are attributed to the C-H stretching vibrations of alkyl groups. The peak around 1450 cm^{-1} is due to C-H deformation vibrations of alkyl groups. In the case of the Fe-assisted sample, these alkyl peak were slightly more intense than those corresponding to the conventionally liquefacted sample, suggesting that dehydration and hydrodeoxygenation reactions are promoted by Fe. Both samples exhibited absorptions in the 1700 cm^{-1} region, consistent with C=O stretching vibrations and suggestive of the presence of carbonyl compounds. The peak at 1600 cm^{-1} is attributed to aromatic C=C stretching or quinone C=O stretching. The peak at 1250 cm^{-1} and 1050 cm^{-1} arising from C-O stretching indicates the presence of alcohols, ethers, esters, or phenols. Overall, peaks between 1700 and 1000 cm^{-1} were unclear in the spectrum of the conventionally liquefacted sample, indicating that this sample is a more complicated mixture than the Fe-assisted sample. The IR spectrum profiles of FDBs are analogous with those of humins or biochars [42-44], suggesting these substances are structurally similar.

3.2.4. Molecular-weight distributions of the freeze-dried WS samples

In order to investigate the molecular-weight distributions of the heavy WS components, the FDB samples were analyzed by GPC, and the differential molecular-weight distribution profiles are displayed in Figure 9, with the average molecular weights listed in Table 5. Molecular weight distributions were measured in poly(ethylene glycol) equivalents.

Figure 9 reveals that a group of compounds with molecular weights distributed in the 100 to 500 range can be separated by the freeze-drying method. A molecular weight of 500 corresponds to a trimer of sugars or monomeric lignin units [45]. The mass-average molecular weight (Mw) was around 250 for both Fe-assisted and conventional samples. We conclude, therefore, that the heavy WS components are composed of oligomers containing polar functional groups (OH, COOH), rather than polymers; these components are formed by the denaturation of oligomeric sugars or lignin that were incompletely decomposed during the hydrothermal process, or by the condensation of low molecular-weight products. Considering that humins are produced through similar pathways [44] but have large molecular weight distributions [46] and low solubilities in water, the heavy WS components are considered to be a precursor of humins [47]. As shown in Table 4, the proportion of the heavy WS components contained in the crude WS fraction prepared by Fe-assisted hydrothermal decomposition was lower than that of the sample prepared by conventional hydrothermal decomposition. In addition, the molecular-weight profiles of the two FDB samples are slightly different (Figure 9). These results indicate that the reaction route changes

following the addition of Fe. A likely explanation is that Fe accelerates biomass decomposition and/or suppresses the re-condensation of the decomposition products [14]. As discussed above, detailed analyses of the light and heavy WS components verify that Fe has a remarkable effect on the hydrothermal liquefaction of biomass.

3.3. Catalytic cracking of the WS-VF and WS-FDB

Catalytic cracking of the WS fractions obtained from EFBs produced hydrocarbons such as olefins, as well as benzene, toluene, and xylenes (BTX). The WS fraction obtained by the Fe-assisted hydrothermal decomposition of the EFB exhibited a higher yield of hydrocarbons than that obtained by conventional hydrothermal decomposition [14], which we consider to be due to the higher concentrations of light compounds in the Fe-assisted WS fraction. In order to verify this hypothesis, cracking experiments were carried out on the VF and FDB of the Fe-assisted WS fraction, the results which were compared with those of the crude WS fraction and displayed in Table 6.

As expected, the VF produced cracking products in higher yields. When the unseparated WS sample was used, the carbon balance between the fed carbon and the product was poor, whereas when the VF was used the carbon balance was almost 90%. On the other hand, when the FDB was used, the hydrocarbon yield was lower and the carbon balance decreased to less than 50%.

The low carbon balances observed for the crude WS fraction and the FDB are ascribed to non-volatile (heavy) compounds that become carbonized and fixed as coke in the vaporizer of the reactor. Therefore, in

order to improve the hydrocarbon yield, it is important that the proportion of the light WS components in the crude WS fraction is increased. The development of a catalyst that promotes decomposition and suppresses re-condensation of the WS components is therefore required.

3.4. Summary of the product distributions obtained by hydrothermal liquefaction

Figure 10 provides an overview of the products obtained by hydrothermal liquefaction including those that are not in WS fractions. By quantitatively analyzing the WS fractions, the changes in product distribution due to the addition of Fe become clear. We previously reported that the addition of Fe significantly increases the proportion of the WS fraction. Herein, we confirmed that the proportion of highly volatile compounds (light WS components) had increased remarkably. On the other hand, the acetone-soluble and water-insoluble (WI) fractions, and the solid residues (SRs), which are considered to be complex polymeric compounds, both decreased. As a result, the addition of Fe to the system resulted in a shift of the molecular-weight distribution of the products to a lower average value.

4. Conclusion

In this study, we developed a method for the quantification of the WS fraction from the hydrothermal liquefaction of biomass. The composition of the light WS components was revealed through a combination of GC–MS (for identification) and GC–FID (for quantification). An empirical RRF estimation method, based on the ECN concept, was developed to quantify compounds with unknown FID sensitivities. A good

correlation was obtained between the experimental and the calculated RRF values through the optimization of the ECN contribution coefficient (Cnt) of each analyte functional group against the analysis data of 32 standard samples. GC analyses of the WS fractions revealed that the addition of Fe during hydrothermal liquefaction altered the product distribution and increased the yield of the light WS components.

Heavy WS components were isolated by removing water and the light WS components by freeze-drying, which enabled various analyses to be performed. Quantitative information on the heavy WS components was obtained by elemental analysis and GPC, while qualitative information was provided by FT-IR spectroscopy. These results suggest that the addition of Fe affects the composition and structure of the heavy WS components.

Catalytic cracking of each WS fraction using the HZSM-5 zeolite was investigated under the same conditions, which revealed that the light WS components gave high yields of olefins. These results confirm the importance of improving the yield of the light WS components, and provide guidance for improving the economics of the hydrothermal liquefaction and cracking system. The development of improved catalysts and the optimization of the reaction condition are currently in progress.

Acknowledgements

The authors gratefully acknowledge financial support from Nippon Shokubai Co., Ltd. We would like to thank the Analysis Technology Center of Nippon Shokubai for GC–MS analysis.

Funding

This research did not receive any specific grant from funding agencies in the public, commercial, or not-for-profit sectors.

Declarations of interest

None

References

[1] S. Xiu, A. Shahbazi, Bio-oil production and upgrading research: A review, Renew. Sust. Energy Rev. 16 (2012) 4406–4414. http://dx.doi.org/10.1016/j.rser.2012.04.028

[2] G. Kumar, S. Shobana, W.-H. Chen, Q.-V. Bach, S.-H. Kim, A.E. Atabani, J.-S. Chang, A review of thermochemical conversion of microalgal biomass for biofuels: chemistry and processes, Green Chem. 19 (2017) 44–67. http://dx.doi.org/10.1039/c6gc01937d

[3] A.A. Peterson, F. Vogel, R.P. Lachance, M. Fröling, J.M.J. Antal, J.W. Tester, Thermochemical biofuel production in hydrothermal media: A review of sub- and supercritical water technologies, Energy Environmen. Sci. 1 (2008) 32–65. http://dx.doi.org/10.1039/b810100k

[4] J. Akhtar, N.A.S. Amin, A review on process conditions for optimum bio-oil yield in hydrothermal liquefaction of biomass, Renew. Sust. Energy Rev. 15 (2011) 1615–1624. http://dx.doi.org/10.1016/j.rser.2010.11.054

[5] Y. Xue, H. Chen, W. Zhao, C. Yang, P. Ma, S. Han, A review on the operating conditions of producing bio-oil from hydrothermal liquefaction of biomass, Int. J. Energy Res. 40 (2016) 865–877. http://dx.doi.org/10.1002/er.3473

[6] S.S. Toor, L. Rosendahl, A. Rudolf, Hydrothermal liquefaction of biomass: A review of subcritical water technologies, Energy 36 (2011) 2328–2342. http://dx.doi.org/10.1016/j.energy.2011.03.013

[7] P. Sun, M. Heng, S.-H. Sun, J. Chen, Analysis of liquid and solid products from liquefaction of paulownia in hot-compressed water, Energy Convers. Manage. 52 (2011) 924–933.

http://dx.doi.org/10.1016/j.enconman.2010.08.020

[8] Y. Kurimoto, M. Takeda, A. Koizumi, S. Yamauchi, S. Doi, Y. Tamura, Mechanical properties of polyurethane films prepared from liquefied wood with polymeric MDI, Bioresour. Technol. 74 (2000) 151–157. http://dx.doi.org/10.1016/s0960-8524(00)00009-2

[9] E.A. Ramos-Tercero, A. Bertucco, D.W.F. Brilman, Process water recycle in hydrothermal liquefaction of microalgae to enhance bio-oil yield, Energy Fuels 29 (2015) 2422–2430. http://dx.doi.org/10.1021/ef502773w

[10] R. Cherad, J.A. Onwudili, P. Biller, P.T. Williams, A.B. Ross, Hydrogen production from the catalytic supercritical water gasification of process water generated from hydrothermal liquefaction of microalgae, Fuel 166 (2016) 24–28. http://dx.doi.org/10.1016/j.fuel.2015.10.088

[11] G. Tommaso, W.T. Chen, P. Li, L. Schideman, Y. Zhang, Chemical characterization and anaerobic biodegradability of hydrothermal liquefaction aqueous products from mixed-culture wastewater algae, Bioresour. Technol. 178 (2015) 139–146. http://dx.doi.org/10.1016/j.biortech.2014.10.011

[12] K. Wu, M. Yang, Y. Chen, W. Pu, H. Hu, Y. Wu, Aqueous-phase ketonization of acetic acid over Zr/Mn mixed oxides, AlChE J. 63 (2017) 2958–2967. http://dx.doi.org/10.1002/aic.15687

[13] S. Zou, Y. Wu, M. Yang, I. Kaleem, J. Zhou, C. Li, J. Tong, Response to “Comments on ‘Thermochemical catalytic liquefaction of the marine microalgae *Duanaliella tertiolecta* and characterization of bio-oils’ by Zou et al.”, Energy Fuels 24 (2010) 3710–3712. http://dx.doi.org/10.1021/ef9012664

[14] Y. Miyata, K. Sagata, M. Hirose, Y. Yamazaki, A. Nishimura, N. Okuda, Y. Arita, Y. Hirano, Y. Kita, Fe-assisted hydrothermal liquefaction of lignocellulosic biomass for producing high-grade bio-oil, ACS Sustain. Chem. Eng. 5 (2017) 3562–3569. http://dx.doi.org/10.1021/acssuschemeng.7b00381

[15] S.R. Villadsen, L. Dithmer, R. Forsberg, J. Becker, A. Rudolf, S.B. Iversen, B.B. Iversen, M. Glasius, Development and application of chemical analysis methods for investigation of bio-oils and aqueous phase from hydrothermal liquefaction of biomass, Energy Fuels 26 (2012) 6988–6998. http://dx.doi.org/10.1021/ef300954e

[16] E. Panisko, T. Wietsma, T. Lemmon, K. Albrecht, D. Howe, Characterization of the aqueous fractions from hydrotreatment and hydrothermal liquefaction of lignocellulosic feedstocks, Biomass Bioenergy 74 (2015) 162–171. http://dx.doi.org/10.1016/j.biombioe.2015.01.011

[17] B. Maddi, E. Panisko, K. Albrecht, D. Howe, Qualitative characterization of the aqueous fraction from hydrothermal liquefaction of algae using 2D gas chromatography with time-of-flight mass spectrometry, J. Vis. Exp. (2016) 1–11. http://dx.doi.org/10.3791/53634

[18] R.B. Madsen, P. Biller, M.M. Jensen, J. Becker, B.B. Iversen, M. Glasius, Predicting the chemical composition of aqueous phase from hydrothermal liquefaction of model compounds and biomasses, Energy Fuels 30 (2016) 10470–10483. http://dx.doi.org/10.1021/acs.energyfuels.6b02007

[19] B. Maddi, E. Panisko, T. Wietsma, T. Lemmon, M. Swita, K. Albrecht, D. Howe, Quantitative

characterization of aqueous byproducts from hydrothermal liquefaction of municipal wastes, food industry wastes, and biomass grown on waste, ACS Sustain. Chem. Eng. 5 (2017) 2205–2214. http://dx.doi.org/10.1021/acssuschemeng.6b02367

[20] J.C. Sternberg, W.S. Gallaway, D.T.L. Jones, Mechanism of response of flame ionization detectors, in: N. Brenner, J.E. Callen, M.D. Weiss (Eds.), Gas Chromatography, Academic Press, New York, 1962, pp. 231–267.

[21] E. Cicchetti, P. Merle, A. Chaintreau, Quantitation in gas chromatography: usual practices and performances of a response factor database, Flavour Fragr. J. 23 (2008) 450–459. http://dx.doi.org/10.1002/ffj.1906

[22] J.-Y. de Saint Laumer, S. Leocata, E. Tissot, L. Baroux, D.M. Kampf, P. Merle, A. Boschung, M. Seyfried, A. Chaintreau, Prediction of gas chromatography with flame ionization detection response factors: algorithm improvement, extension to silylated compounds, and application to the quantification of metabolites, J. Sep. Sci. 38 (2015) 3209–3217. http://dx.doi.org/10.1002/jssc.201500106

[23] E. Tissot, S. Rochat, C. Debonneville, A. Chaintreau, Rapid GC–FID quantification technique without authentic samples using predicted response factors, Flavour Fragr. J. 27 (2012) 290–296. http://dx.doi.org/10.1002/ffj.3098

[24] J.-Y. de Saint Laumer, E. Cicchetti, P. Merle, J. Egger, A. Chaintreau, Quantification in gas chromatography: prediction of flame ionization detector response factors from combustion

enthalpies and molecular structures, Anal. Chem. 82 (2010) 6457–6462. http://dx.doi.org/10.1021/ac1006574

[25] J.J. Filippi, E. Belhassen, N. Baldovini, H. Brevard, U.J. Meierhenrich, Qualitative and quantitative analysis of vetiver essential oils by comprehensive two-dimensional gas chromatography and comprehensive two-dimensional gas chromatography/mass spectrometry, J. Chromatogr. A 1288 (2013) 127–148. http://dx.doi.org/10.1016/j.chroma.2013.03.002

[26] T. Cachet, H. Brevard, A. Chaintreau, J. Demyttenaere, L. French, K. Gassenmeier, D. Joulain, T. Koenig, H. Leijs, P. Liddle, G. Loesing, M. Marchant, Ph. Merle, K. Saito, C. Schippa, F. Sekiya, T. Smith, IOFI recommended practice for the use of predicted relative-response factors for the rapid quantification of volatile flavouring compounds by GC–FID, Flavour Fragr. J. 31 (2016) 191–194. http://dx.doi.org/10.1002/ffj.3311

[27] U. Neuenschwander, A. Negron, K.F. Jensen, A clock reaction based on molybdenum blue, J. Phys. Chem. A 117 (2013) 4343–4351. http://dx.doi.org/10.1021/jp400879d

[28] D.L. Dalluge, T. Daugaard, P. Johnston, N. Kuzhiyil, M.M. Wright, R.C. Brown, Continuous production of sugars from pyrolysis of acid-infused lignocellulosic biomass, Green Chem. 16 (2014) 4144–4155. http://dx.doi.org/10.1039/c4gc00602j

[29] R. Olcese, V. Carré, F. Aubriet, A. Dufour, Selectivity of bio-oils catalytic hydrotreatment assessed by petroleomic and GC*GC/MS–FID analysis, Energy Fuels 27 (2013) 2135–2145. http://dx.doi.org/10.1021/ef302145g

[30] M.R. Djokic, T. Dijkmans, G. Yildiz, W. Prins, K.M. Van Geem, Quantitative analysis of crude and stabilized bio-oils by comprehensive two-dimensional gas-chromatography, J. Chromatogr. A 1257 (2012) 131–140. http://dx.doi.org/10.1016/j.chroma.2012.07.035

[31] C. Michailof, T. Sfetsas, S. Stefanidis, K. Kalogiannis, G. Theodoridis, A. Lappas, Quantitative and qualitative analysis of hemicellulose, cellulose and lignin bio-oils by comprehensive two-dimensional gas chromatography with time-of-flight mass spectrometry, J. Chromatogr. A 1369 (2014) 147–160. http://dx.doi.org/10.1016/j.chroma.2014.10.020

[32] A. Undri, M. Abou-Zaid, C. Briens, F. Berruti, L. Rosi, M. Bartoli, M. Frediani, P. Frediani, A simple procedure for chromatographic analysis of bio-oils from pyrolysis, J. Anal. Appl. Pyrolysis 114 (2015) 208–221. http://dx.doi.org/10.1016/j.jaap.2015.05.019

[33] G. Addis, R. Baskaran, M. Raju, A. Ushadevi, Z. Asfaw, Z. Woldu, V. Baskaran, Effect of blanching and drying process on carotenoids composition of underutilized Ethiopian (*Coccinia grandis* L. Voigt) and Indian (*Trigonella foenum-graecum* L.) green leafy vegetables, J. Food Process. Preserv. 33 (2009) 744–762. http://dx.doi.org/10.1111/j.1745-4549.2008.00308.x

[34] L. Tejada, M. Vioque, R. Gómez, J. Fernández-Salguero, Effect of lyophilisation, refrigerated storage and frozen storage on the coagulant activity and microbiological quality of *Cynara cardunculus* L. extracts, J. Sci. Food Agric. 88 (2008) 1301–1306. http://dx.doi.org/10.1002/jsfa.3193

[35] C.M. Michailof, K.G. Kalogiannis, T. Sfetsas, D.T. Patiaka, A.A. Lappas, Advanced analytical

techniques for bio-oil characterization, WIREs Energy Environ. 5 (2016) 614–639. http://dx.doi.org/10.1002/wene.208

[36] J.E. Szulejko, Y.H. Kim, K.H. Kim, Method to predict gas chromatographic response factors for the trace-level analysis of volatile organic compounds based on the effective carbon number concept, J. Sep. Sci. 36 (2013) 3356–3365. http://dx.doi.org/10.1002/jssc.201300543

[37] P. O'Connor, Chapter 1 - A General Introduction to Biomass Utilization Possibilities, in: K.S. Triantafyllidis, A.A. Lappas, M. Stöcker (Eds.), The Role of Catalysis for the Sustainable Production of Bio-fuels and Bio-chemicals, Elsevier, Amsterdam, 2013, pp. 1–25. http://dx.doi.org/10.1016/b978-0-444-56330-9.00001-2

[38] N.Y. Chen, T.F. Degnan, L.R. Koenig, Liquid fuel from carbohydrates, Chemtech 16 (1986) 506–511.

[39] T.P. Vispute, H.Y. Zhang, A. Sanna, R. Xiao, G.W. Huber, Renewable chemical commodity feedstocks from integrated catalytic processing of pyrolysis oils, Science 330 (2010) 1222–1227. http://dx.doi.org/10.1126/science.1194218

[40] Y. Mei, R. Liu, Effect of temperature of ceramic hot vapor filter in a fluidized bed reactor on chemical composition and structure of bio-oil and reaction mechanism of pine sawdust fast pyrolysis, Fuel Process. Technol. 161 (2017) 204–219. http://dx.doi.org/10.1016/j.fuproc.2016.09.008

[41] S. Sahoo, C. Chakraborti, P. Behera, S. Mishra, FTIR and Raman spectroscopic investigations of a

norfloxacin/carbopol934 polymeric suspension, J. Young Pharm. 4 (2012) 138–145. http://dx.doi.org/10.4103/0975-1483.100017

[42] S. Zhang, L. Yuan, W. Li, Z. Lin, Y. Li, S. Hu, B. Zhao, Characterization of pH-fractionated humic acids derived from Chinese weathered coal, Chemosphere 166 (2017) 334–342. http://dx.doi.org/10.1016/j.chemosphere.2016.09.095

[43] C.B. Rasrendra, M. Windt, Y. Wang, S. Adisasmito, I.G.B.N. Makertihartha, E.R.H. van Eck, D. Meier, H.J. Heeres, Experimental studies on the pyrolysis of humins from the acid-catalysed dehydration of C6-sugars, J. Anal. Appl. Pyrolysis 104 (2013) 299–307. http://dx.doi.org/10.1016/j.jaap.2013.07.003

[44] M. Sevilla, A.B. Fuertes, The production of carbon materials by hydrothermal carbonization of cellulose, Carbon 47 (2009) 2281–2289. http://dx.doi.org/10.1016/j.carbon.2009.04.026

[45] J. Zakzeski, P.C.A. Bruijnincx, A.L. Jongerius, B.M. Weckhuysen, The catalytic valorization of lignin for the production of renewable chemicals, Chem. Rev. 110 (2010) 3552–3599. http://dx.doi.org/10.1021/cr900354u

[46] G. Almendros, J. Sanz, L. Sobrados, Characterization of synthetic carbohydrate-derived humic-like polymers, Sci. Total Environ. 81-82 (1989) 91–98. http://dx.doi.org/10.1016/0048-9697(89)90114-9

[47] I. van Zandvoort, Y. Wang, C.B. Rasrendra, E.R. van Eck, P.C. Bruijnincx, H.J. Heeres, B.M. Weckhuysen, Formation, molecular structure, and morphology of humins in biomass conversion:

influence of feedstock and processing conditions, ChemSusChem 6 (2013) 1745–1758. http://dx.doi.org/10.1002/cssc.201300332

Tables

Table 1. Results of Fe-assisted and conventional hydrothermal liquefaction of EFB.[a]

Reaction system	Carbon yield (%C)					pH of the WS fraction
	Gas	WS	WI	SR	total	
Fe-assisted	4%	56%	23%	10%	93%	4.5
Conventional	7%	33%	38%	17%	95%	3.4

[a] Reaction conditions: EFB = 4 g, H_2O = 40 g, Fe = 6.256 g or 0 g, initial pressure = 1.0 MPa (N_2), temperature = 300 °C, time = 10 min. Yields were calculated based on the carbon content of raw EFB.

Table 2. Optimized Cnt and RRF values of authentic samples.

Functional group	Cnt
C	1.000
H	-0.075
O	0.226
C(alkyl)	0.037
C(olefin)	-0.208
C(aromatic)	-0.010
C=O(ketone)	-1.389
C=O(aldehyde)	-0.753
C=O(acid)	-1.417
O(ether)	-0.906
OH(1°)	-0.651
OH(2°)	-0.754
OH(3°)	0.567
OH(Aryl)	-0.857

Authentic samples	RRF_{calc}	RRF_{found}
Cyclopentanone	2.18	2.26
3-Hydroxy-2-butanone	1.12	1.19
1-hydroxy-2-Propanone	0.76	0.63
Acetic acid	0.70	0.73
Propanoic acid	1.21	1.23
Propyleneglycol	1.11	1.18
1,2-Ethanediol	0.68	0.79
1,2-Butanediol	1.47	1.52
4-Oxopentanoic acid	1.11	1.12
5-hydroxymethyl-2-furaldehyde	1.34	1.34
Phenol	2.80	2.70
Guaiacol	2.21	2.23
Cyclohexanone	2.35	2.40
Propanol	1.88	1.89
Cyclopentanol	2.45	2.31
Cyclohexanol	2.59	2.49
Furfural	1.50	1.53
2-Butanone	1.76	1.90
1,2-Pentanediol	1.73	1.59
1,2-Hexanediol	1.93	1.93
1,2-Cyclohexanediol	1.99	2.09
2,3-Butanediol	1.41	1.43
1,4-Butanediol	1.53	1.63
Syringol	1.85	1.98
Methyl DL-2-Hydroxy-3-butenoate	1.20	1.12
Methyl p-Hydroxybenzoate	2.06	2.01
Cinnamaldehyde	3.03	2.96
Syringaldehyde	1.71	1.74
3-Phenyl-2-propen-1-ol	2.97	3.04
Vanillin	1.97	1.98
tert-Butyl alcohol	2.34	2.32
tert-Amyl alcohol	2.36	2.38

Table 3. Quantitative results from the GC analysis of the WS fraction prepared by the hydrothermal liquefaction of EFB.[a]

			Molecular		RRF		Fe-assisted		Conventional	
R.T.	Compound name	Formula	Weight	Classification	Found/Calculated	Value	Area	Yield (%C)	Area	Yield (%C)
5.841	2-Methoxyethanol	$C_3H_8O_2$	76.09	Internal standard			30197		28442	
5.909	Cyclopentanone	C_5H_8O	84.12	ketone	Found	2.22	4876	0.50%	3454	0.09%
7.567	3-Hydroxy-2-butanone	$C_4H_8O_2$	88.11	hydroxyketone	Found	1.41	24176	2.98%	5207	0.17%
7.803	Hydroxyacetone	$C_3H_6O_2$	74.08	hydroxyketone	Found	0.67	31393	7.24%	11888	0.65%
8.437	2-Methyl-3-hexanone	$C_7H_{14}O$	114.19	ketone	Calculated	2.37	18513	1.83%	1482	0.04%
8.677	2-Methyl-2-cyclopenten-1-one	C_6H_8O	96.13	ketone	Calculated	2.21	30748	3.32%	11106	0.08%
8.846	1-Hydroxy-2-butanone	$C_4H_8O_2$	88.11	hydroxyketone	Calculated	1.18	10684	1.57%	6204	0.24%
8.86	Tetrahydro-2-(methoxymethyl)furan	$C_6H_{12}O_2$	116.16	ether	Calculated	1.85			2893	0.08%
9.439	Cyclohexanol	$C_6H_{12}O$	100.16	alcohol	Found	2.49	2865	0.26%		
9.68	2-pentyl methoxyacetate	$C_8H_{16}O_3$	160.21	ester/ether	Calculated	1.83	5612	0.59%		
9.776	4-Heptanol	$C_7H_{16}O$	116.20	alcohol	Calculated	2.57	7154	0.64%		
9.912	1-Hydroxy-2-pentanone	$C_5H_{10}O_2$	102.13	hydroxyketone	Calculated	1.49	8822	1.11%		
10.001	Acetic acid	$C_2H_4O_2$	60.05	carboxylic acid	Found	0.71	24852	4.49%	137968	5.77%
10.143	Furfural	$C_5H_4O_2$	96.08	ether/aldehyde	Found	1.53			9321	0.26%
10.629	Tetrahydro-2-furanmethanol	$C_5H_{10}O_2$	102.13	alcohol/ether	Calculated	1.76	2388	0.25%		
10.695	2,5-Hexanedione	$C_6H_{10}O_2$	114.14	ketone	Calculated	1.46			4304	0.16%
11.155	Propanoic acid	$C_3H_6O_2$	74.08	carboxylic acid	Found	1.16	3428	0.46%	9881	0.32%
12.03	1-Ethoxy-3-pentanol	$C_7H_{16}O_2$	132.20	alcohol/ether	Calculated	1.98	4415	0.45%		
12.227	1,2-Ethanediol	$C_2H_6O_2$	62.07	alcohol	Found	0.77	2824	0.45%		
12.295	Butyrolactone	$C_4H_6O_2$	86.09	ester	Calculated	1.7	1293	0.14%		
13.928	1,2-Pentanediol	$C_5H_{12}O_2$	104.15	alcohol	Found	1.59			1314	0.04%

14.952	Guaiacol	$C_7H_8O_2$	124.14	ether/phenol	Found	2.11	1787	0.18%	6243	0.15%
16.437	Phenol	C_6H_6O	94.11	phenol	Found	2.63	14854	1.38%	60946	1.48%
18.759	1,1'-[Ethylidenebis(oxy)]bis[2-methyl-propane]	$C_{10}H_{22}O_2$	174.28	ether	Calculated	2.28	4929	0.47%		
18.952	Syringol	$C_8H_{10}O_3$	154.16	ether/phenol	Found	1.97	2655	0.27%	10953	0.27%
19.423	4-Oxopentanoic acid,	$C_5H_8O_3$	116.12	ketone/carboxylic acid	Found	0.98			5657	0.24%
	total							29%		10%

[a] Yields were calculated based on the carbon content of the raw EFB.

Table 4. Mass balances and carbon balances following freeze-dry separations of the crude WS fractions.

	Mass balance (wt%)[a]			Carbon balance (%C)[b]		
	WS-FDB	WS-VF	total	WS-FDB	WS-VF	total
Fe-assisted	2%	97%	99%	46%	52%	98%
Conventional	2%	98%	100%	68%	32%	100%

[a] Calculated based on the weight of the freeze-dried crude WS fraction.

[b] Calculated based on the carbon content of the freeze-dried crude WS fraction.

Table 5. Average molecular weights of WS-FDB.[a]

	M_n	M_w	M_z
Fe-assisted	219	277	321
Conventional	194	252	299

[a] Poly(ethylene glycol) equivalent.

Table 6. Catalytic cracking of WS-VF and WS-FDB and comparisons with the crude WS fraction.[a]

	Carbon yields (%C)													Carbon balance (%C)
	olefins				BTX	olefin + BTX	Alkanes			COx			Water solubles[b]	
	C_2	C_3	C_4	Sum	Sum	Sum	C_1	$C_{2\text{-}5}$	Sum	CO	CO_2	Sum		
Crude WS	12	14	2	28	7	35	3	2	5	9	4	13	13	66
WS-VF	17	20	4	41	8	49	3	3	6	13	9	22	11	88
WS-FDB	4	6	1	11	3	14	2	1	3	5	4	9	24	50

[a] Preparation conditions of WS: EFB = 4 g, H_2O = 40 g, Fe = 6.256 g or 0 g, initial pressure = 1.0 MPa (N_2), temperature = 300 °C, time = 10 min.

Cracking conditions: HZSM-5 = 3.3 g (6 mL, d = 0.55), WS feed = weight hourly space velocity of 1.1 h^{-1}, N_2 = 50 mL/min, temperature = 300 °C. Yields were calculated based on the fed-in WS fraction.

[b] Collected carbon in the gas wash bottle.

Figures

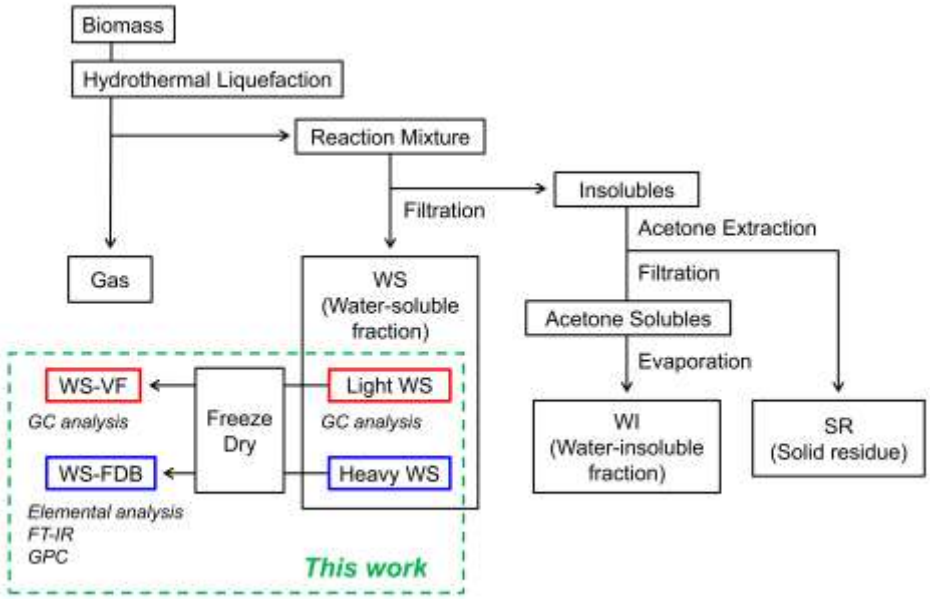

Figure 1. Products from the hydrothermal liquefaction of biomass and an overview of our analysis strategy.

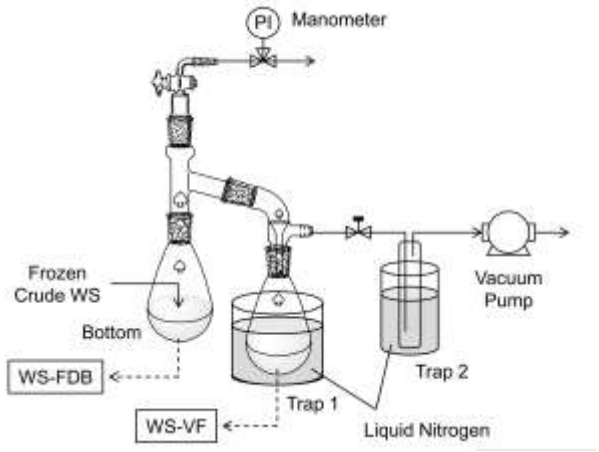

Figure 2. Schematic layout of the freeze-drying apparatus.

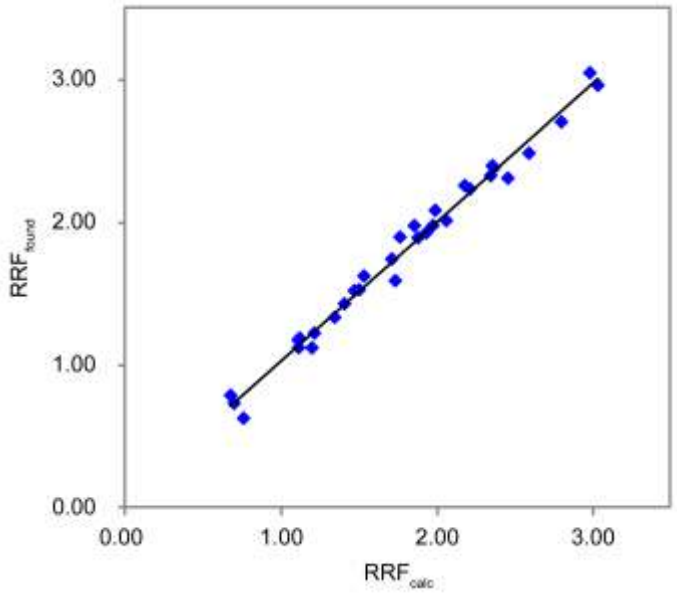

Figure 3. Comparison between RRF_{found} and optimized RRF_{calc} for authentic samples.

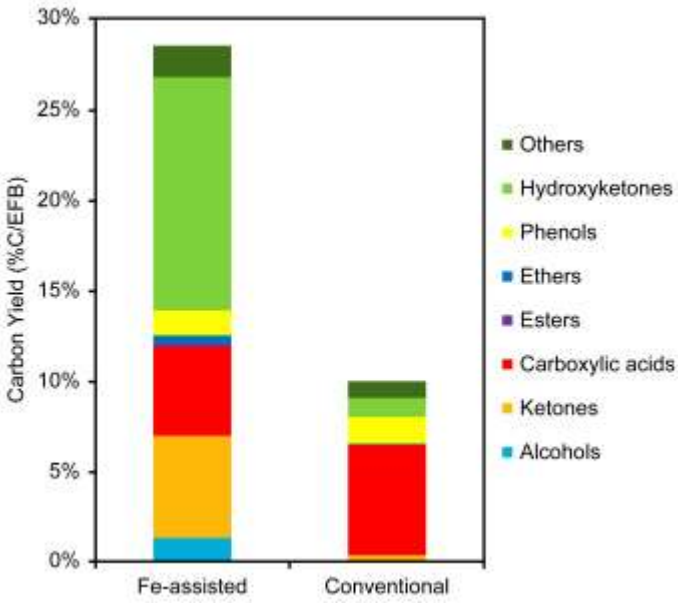

Figure 4. Distributions of compounds in the light WS components.

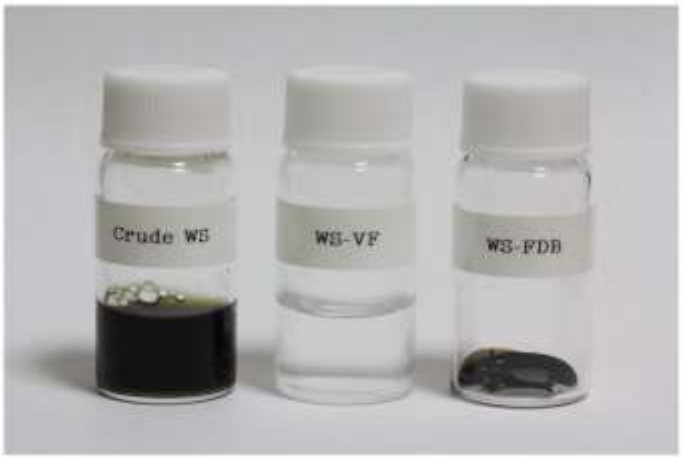

Figure 5. Photographic images before and after the freeze-dry separation of the WS fraction. From left to right: Crude WS fraction, volatile fraction, freeze-dried bottom.

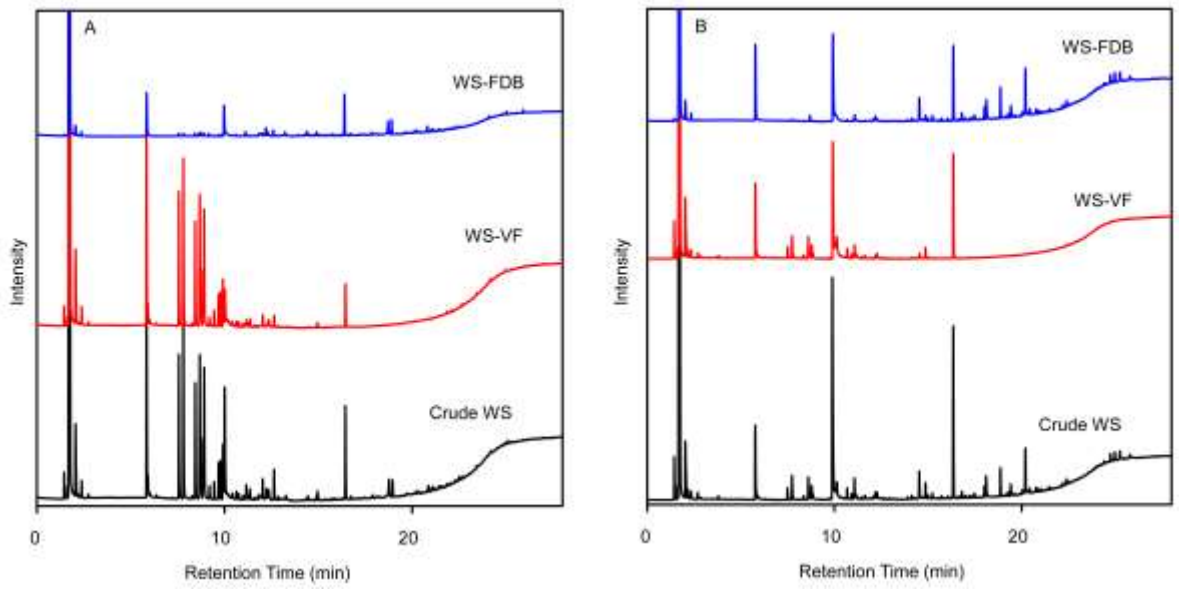

Figure 6. Comparisons of the GC–FID chromatogram of the crude WS fraction with those of WS-VF and WS-FDB; (a) Fe-assisted, (b) conventional.

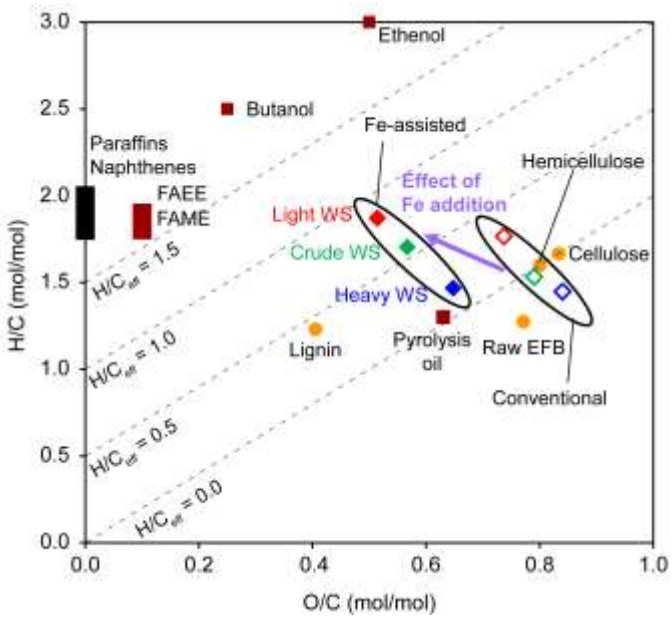

Figure 7. van Krevelen diagram of the WS fractions, biomass feedstocks, biomass-derived chemicals, and petrochemicals.

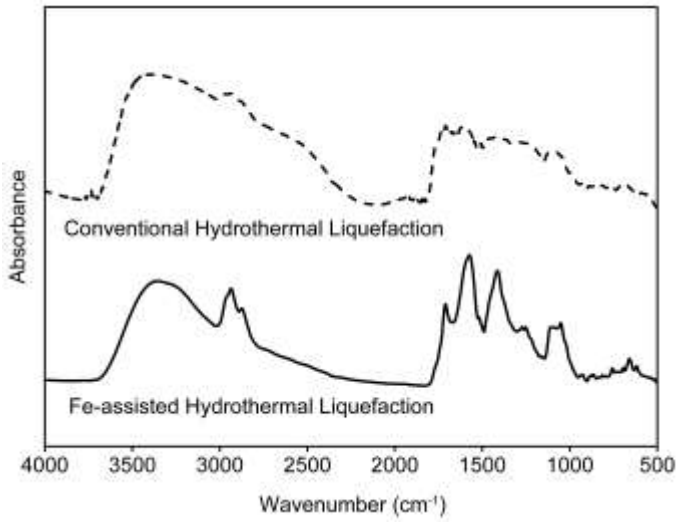

Figure 8. FT-IR spectra of WS-FDB.

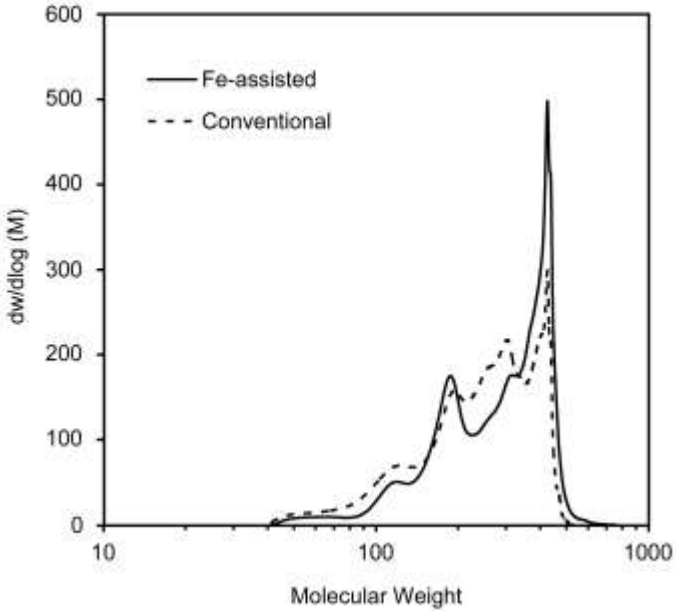

Figure 9. Molecular weight distributions of WS-FDB (poly(ethylene glycol) equivalents).

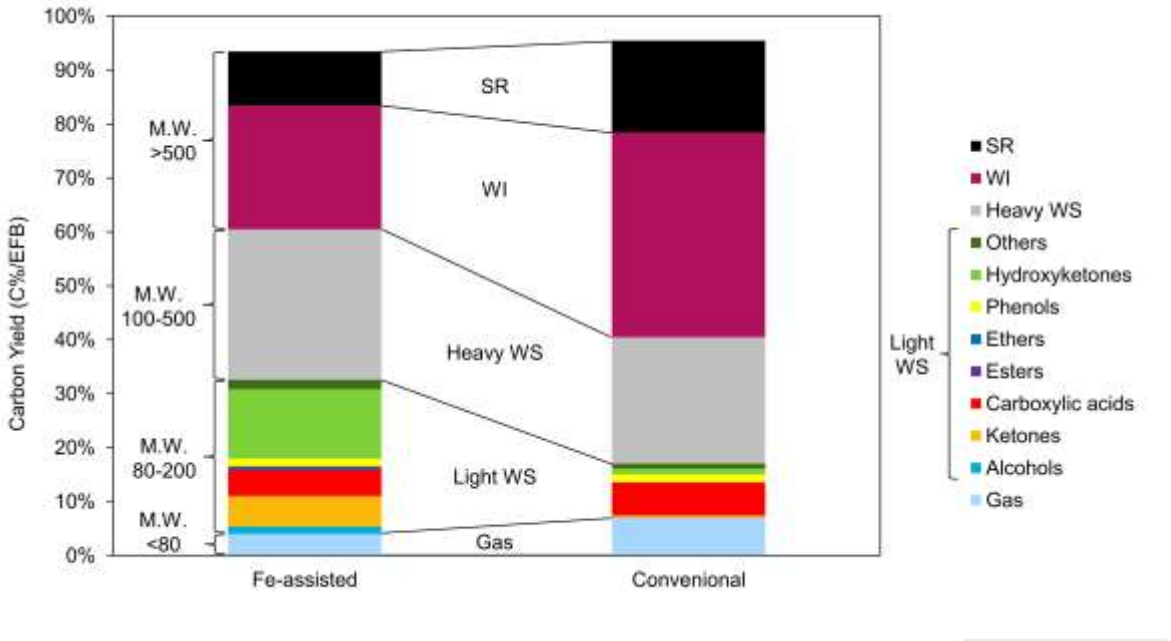

Figure 10. Summary of product yields from the hydrothermal liquefaction of EFB.